Original Article

Electroacupuncture ameliorates surgery-induced spatial memory deficits by promoting mitophagy in rats

Jian Guo[1,2,3#], Kun Niu[2,4#], Bao-Feng Ma[1,2], Li-Na Sun[1,2], Qi-Wu Fang[2], Jian-Xiong An[1,2,5]

[1]School of Anesthesiology, Weifang Medical University, Weifang, China; [2]Department of Anesthesiology, Pain and Sleep Medicine, Aviation General Hospital of China Medical University and Beijing Institute of Translational Medicine, Chinese Academy of Sciences, Beijing, China; [3]Department of Anesthesiology, Yan'an People's Hospital, Yan'an, China; [4]Key Laboratory of Carcinogenesis and Translational Research (Ministry of Education/Beijing), Department of Anesthesiology, Peking University Cancer Hospital and Institute, Beijing, China; [5]Department of Anesthesiology, Pain and Sleep Medicine, The Affiliated Hospital of Weifang Medical University, Weifang, China

Contributions: (I) Conception and design: J Guo, K Niu, JX An; (II) Administrative support: JX An; (III) Provision of study materials or patients: QW Fang, JX An; (IV) Collection and assembly of data: J Guo, K Niu, BF Ma, LN Sun; (V) Data analysis and interpretation: J Guo, K Niu, BF Ma, LN Sun; (VI) Manuscript writing: All authors; (VII) Final approval of manuscript: All authors.

[#]These authors contributed equally to this work.

Correspondence to: Jian-Xiong An, MD, PhD. School of Anesthesiology, Weifang Medical University & Department of Anesthesiology, Pain and Sleep Medicine, The Affiliated Hospital of Weifang Medical University, Baotong West St. #7166, Weifang 261053, China. Email: anjianxiong@yeah.net.

Background: This study sought to explore the mechanism underlying the therapeutic effects of electroacupuncture (EA) on spatial memory deficits caused by surgery.

Methods: Hepatic apex resection was performed under propofol-based total intravenous anesthesia. Male Sprague-Dawley rats were subjected to EA treatment or EA + mitochondrial division inhibitor-1 (mdivi-1) treatment once a day for three consecutive days after surgery. The Morris water maze test was used to evaluate the spatial memory of the rats after surgery. Tissue from the hippocampus of each rat was frozen and used for transcriptomic and proteomic analyses to identify potential targets for EA treatment. Western blotting was used to confirm the protein expression levels. The levels of reactive oxygen species (ROS) and adenosine triphosphate (ATP) were detected using commercial kits. The rat mitochondria were then isolated, and the activity of mitochondrial complex V was assessed.

Results: EA attenuated surgery-induced spatial memory deficits on postoperative day 3, while these effects were reversed by treatment with the mdivi-1 ($P<0.05$). Ribonucleic acid (RNA)-sequencing revealed that EA upregulated multiple metabolic pathways and the phosphatidylinositol 3-kinas/protein kinase B signaling pathway. The proteomic and western blotting results suggested that the EA treatment substantially downregulated coiled-coil-helix-coiled-coil-helix domain containing 3 (ChChd3) expression in the hippocampus. The EA treatment significantly increased the autophagy-related protein levels, including phosphatase and tensin homolog-induced kinase 1, Parkin, MAP1LC3 (LC3), and Beclin1, and inhibited the production of ROS and inflammatory cytokine interleukin-1β in the hippocampus ($P<0.05$).

Conclusions: These results suggest that EA ameliorates postoperative spatial memory deficits and protects hippocampus from oxidative stress and inflammation through enhanced autophagy in an animal model of perioperative neurocognitive disorders (PNDs).

Keywords: Perioperative neurocognitive disorders (PNDs); electroacupuncture (EA); coiled-coil-helix-coiled-coil-helix domain containing 3 (ChChd3); reactive oxygen species (ROS); hippocampus

Submitted Nov 15, 2022. Accepted for publication Jan 10, 2023. Published online Jan 31, 2023.
doi: 10.21037/atm-22-6262
View this article at: https://dx.doi.org/10.21037/atm-22-6262

Introduction

Perioperative neurocognitive disorder (PND) is a common complication after surgery, which manifests as an acute neuropsychiatric state with symptoms, including memory deficits, disorientation, and abnormal abstract thinking and social behaviors (1). The prevalence of PND in patients has been reported to be 29% at 3 months and 33.6% at 12 months after surgery (1). In addition to advanced age, the main risk factors for PND include a low education level, pre-existing cognitive impairment, several poor health conditions, and the duration of the surgery (2). Although multiple factors may contribute to the development of PND, surgery trauma but not anesthesia is a main factor to exacerbate the disease (3). PND results in increased morbidity and mortality, longer hospitalization, and increased health care costs (1). The pathogenesis of PND is not fully understood, but it has been shown to involve oxidative stress, neuroinflammation, mitochondrial dysfunction, blood-brain barrier damage, impaired synaptic function, and a lack of neuro-nutritional support (4). Currently, no effective measures for preventing and treating PND are available.

Mitophagy, a selective autophagy of mitochondria, is a key mechanism that mediates the removal of aged, damaged, or excessive mitochondria to maintain mitochondrial homeostasis for neuron survival (5,6). Reactive oxygen species (ROS) are mainly produced in the mitochondria, and mitochondrial dysfunction may lead to aberrant ROS production (7-9). Autophagy is widely present in eukaryotic cells (10). A number of neurological disorders were associated with autophagy (11). Neurons appear to be particularly dependent on autophagy, and the activation of autophagy ameliorates cortical and hippocampal neuron apoptosis (12). Autophagy dysfunction has been reported to be involved in anesthetic-induced cognitive deficits in aged rats (13). Autophagy has been shown to play a protective role in some neurodegenerative disorders, and the regulation of autophagy has been recognized as an important therapeutic strategy for the treatment of such diseases (14). Phosphatase and tensin homolog-induced kinase (PINK1)-Parkin-mediated mitochondrial autophagy is responsible for the deliberate segregation and removal of damaged mitochondria. Previous studies have shown that impaired autophagic flux in the hippocampus leads to cognitive impairment (15,16). To date, few studies have investigated the association between autophagy and the development of PND.

Acupuncture is a traditional Chinese medical therapy that involves the insertion of needles into specific acupuncture points on the patient's body. Electroacupuncture (EA) is a form of acupuncture therapy that combines traditional acupuncture with electrical stimulation. EA has been accepted by researchers as an effective treatment for various diseases, including cognitive dysfunction (17,18). A clinical study has shown that EA was effective at relieving cognitive impairment and related pathologies following surgery (19). A rodent study showed that EA improved cognitive performance in PND rats by reducing oxidative stress (20). Additionally, EA has been shown to protect against neuronal injury in cerebral ischemia-reperfusion by alleviating nitro/oxidative stress-induced mitochondrial function damage and decreasing damaged mitochondria accumulation via PINK1/Parkin-mediated mitophagy clearance (21). We hypothesized that EA would exert protective effects on spatial memory in a PND rat model by increasing mitophagy and reducing oxidative stress to reduce neuroinflammation. We present the following article in accordance with the ARRIVE reporting checklist (available at https://atm.amegroups.com/article/view/10.21037/atm-22-6262/rc).

Highlight box

Key findings

- Electroacupuncture (EA) ameliorates postoperative spatial memory deficits and protects hippocampus from oxidative stress and inflammation through enhanced autophagy in rats.

What is known and what is new?

- Studies in animals have raised concerns over the possible effects of EA in the treatment of postoperative cognitive disorders.
- In rats, EA improved behavioral tests of cognitive function by increasing mitophagy and reducing oxidative stress.

What is the implication, and what should change now?

- Mitochondrial morphology mediators, such as coiled-coil-helix-coiled-coil-helix domain containing 3 (ChChd3), provide novel targets to treat postoperative neuroinflammation and neurocognitive disorders.

Methods

Ethical approval

This study was approved by the Ethical Committee of the Aviation General Hospital (No. HK-2019-12-17). A protocol was prepared before the study without registration. All the animal experiments were performed in accordance with the National Institutes of Health Guidelines for the Care and Use of Laboratory Animals. Efforts were made to minimize the number of animals used and their suffering.

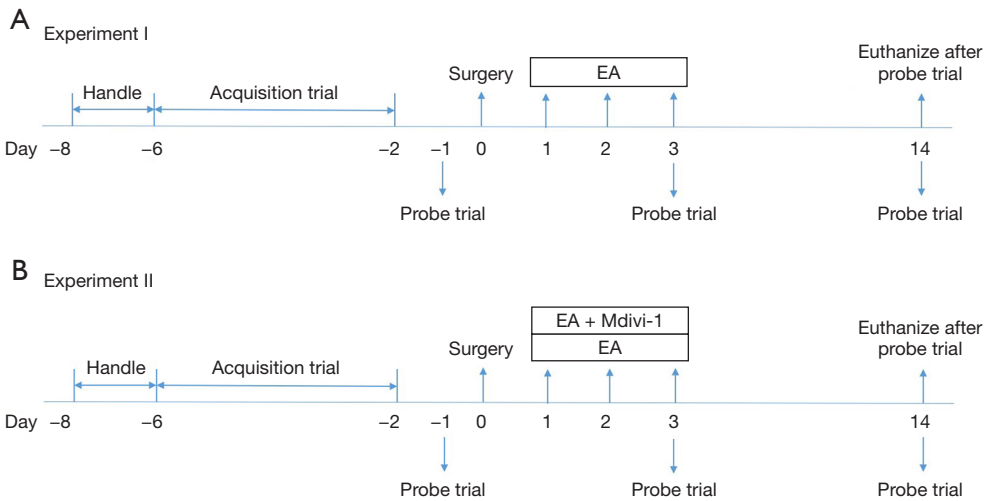

Figure 1 Experimental design. (A) Experiment I: 1 week before surgery, the rats were trained to find a hidden platform in the MWM test. The hepatic apex of the adult rats was then resected. After surgery, the rats were treated with EA daily for 3 consecutive days. Their memory ability was tested at 3 and 14 days postoperatively. The hippocampus tissue was subjected to Western blot and bioinformatics analyses. (B) Experiment II: the rats in the mdivi-1 + EA group were given mdivi-1 and EA therapy concurrently on days 1, 2, and 3. The rest of the method was identical to that of Experiment I. EA, electroacupuncture; MWM, Morris water maze.

Animals

Male Sprague-Dawley (SD) rats (aged 13–14 months and weighing 480–560 g) were provided by the Vital River Laboratory Animal Technology Co. Ltd. (Beijing, China) for this research. Based on our (22-24) and other published data (25,26), rats in this range are equivalent to a human aged greater than 45 years, which is considered one condition for the development of memory impairment following surgery. The rats were housed in cages (of 3–4 rats per cage), kept under a constant temperature (21±1 ℃) and on a 12-h light/dark cycle and had free access to food and water. Food was withheld 18–24 h before surgery. The rats were acclimatized to the laboratory environment for 1 week before the initiation of the experiments.

Experimental design

Experiment I

To verify the roles of EA in the PND rat model in addition to the specific signaling pathways and differentially expressed protein involved in EA, the 48 SD rats were randomly assigned to the following 4 groups using a random number table: (I) the control group (N=12); (II) the model group (N=12); (III) the EA group (N=12); and (IV) the sham EA group (N=12). The sample sizes were estimated empirically. The study investigators were aware of the treatment group allocation. The Morris water maze (MWM) was used to assess spatial memory. Ribonucleic acid (RNA) sequencing, proteomics, and western blot were employed to study the regulation mechanisms of EA. *Figure 1A* shows the design of the experiment schematically.

Experiment II

To study the effects of EA on PINK1/Parkin-mediated mitophagy clearance in a PND rat model, the 48 SD rats were randomly assigned into the following 4 groups using a random number table: (I) the control group (N=12); (II) the model group (N=12); (III) the EA group (N=12); and (IV) the mitochondrial division inhibitor-1 (mdivi-1) + EA group (N=12). The sample sizes were estimated empirically, and the study investigators were aware of the treatment group allocation. We measured the protein expression of the autophagic/mitophagy markers of LC3, Beclin1, PINK1, and Parkin (27). ROS levels and mitochondrial complex V activities were measured to assess oxidative stress and mitochondrial activity. Mdivi-1 was used to investigate whether mitophagy was involved in EA to improve cognition after abdominal surgery in the rats. *Figure 1B* shows the design of the experiment schematically.

Anesthesia and surgery

The PND model was established by resecting the hepatic

apex as previously described (28). Before surgery, each rat was weighed and rested for 30 minutes. The tail was then extended and a 26G-catheter (Covidien, Dublin, Ireland) was placed in the lateral tail vein, and 12.5 mg/kg of intravenous propofol (10 mg/mL, Xi'an Libang Pharmaceutical & Co., Ltd; Xi'an, Shanxi Province, China) was administered to induce anesthesia. The heart rate, respiratory rate and transcutaneous oxygen saturation was monitored. After the initial sedation, anesthesia was maintained in the spontaneously breathing rats during surgery via the continuous infusion of 0.625 mg/kg/min of propofol using a computer-assisted continuous infusion device (Kelly Med TM Syringe Pump, KL605T, Beijing, China). To produce analgesia, 0.1 mg/kg of buprenorphine (0.15 mg/mL, TIPR Pharmaceutical Responsible Co., Ltd., Tianjin, China) was subcutaneously administered immediately after the anesthetic induction. During surgery, a heat light was used to keep the rectal temperature at 37±0.5 ℃. After shaving the abdominal wall, each rat was placed in the supine position and had its abdominal cavity disinfected. The left hepatic duct and artery were ligated with a minor incision in the upper abdominal midline, and the median and left lateral lobes were excised. The procedure was concluded within 10 minutes. The peritoneum and skin were closed with sterile 4–0 chromic gut sutures. Wound infiltration with 0.1% ropivacaine 3 mg/kg (AstraZeneca, Sweden) was used for the postoperative analgesia. The rats in the control group were not given any treatment. The rats in the model group underwent resection of the hepatic apex under the same anesthesia and analgesia conditions as the control group. The rats in the EA group received EA therapy. The rats in the sham EA group were treated the same as the rats in EA group but without electricity. The rats in the mdivi-1 + EA group received both EA therapy and mdivi-1.

EA and mdivi-1 administration

The EA treatment was performed once a day (at 8.00 a.m.) for 3 days after surgery. Alcohol was used to disinfect the skin. As described by Yin *et al.* (29), the acupuncture needles (0.3×13 mm) were inserted horizontally at a depth of 3–4 mm at the following 2 points on the ankle: Sanyinjiao (SP6) and Zusanli (ST36). The location of the SP6 and ST36 was estimated based on the anatomy of the rat model (30). SP6 was located 10 mm above the hindlimb medial malleolus front of the tibia and fibula. ST36 was located at the posterior and lateral side of the knee joint, 5 mm below the capitulum fibulae. An EA instrument (HANS 200A, Nanjing Jisheng Medical Technology Co., Ltd., Nanjing, China) was used to generate stimulation for 30 minutes each day at 1.5 mA. The stimulation frequency of the EA ranged from 2–100 Hz shifting automatically, frequency sweeping; pulse width of 0.6 ms at 2 Hz and 0.1 ms at 100 Hz, each lasting for 3 s) (31). The rats in the sham EA group were restrained in restrainers for 30 minutes with needles at acupoint ST36 and acupoint SP6, but no electrical current was applied. On days 1, 2, and 3 following the surgery, the rats in the mdivi-1 + EA group received mdivi-1 in addition to the treatment received by the EA group. Mdivi-1 (SC8028, Beyotime, Shanghai, China) was dissolved in dimethyl sulfoxide and administered intraperitoneally at 3 mg/kg. It was applied to selectively inhibit mitophagy activation (32).

MWM

The MWM, which is a hippocampus-dependent test, was used to assess the spatial memory of the rats (33). A black metal pool (130 cm in diameter and 35 cm deep) was filled with water (23±2 ℃) to a depth of 25 cm, submerging the 10-cm-diameter escape platform 2 cm below the surface. Non-toxic black ink was used to darken the water. The pool was split equally into the following 4 quadrants: northwest, northeast, southwest, and southeast. Visible cues were affixed to the 4 walls of the pool. The experimental sessions were recorded with a video camera positioned at the middle of the pool's ceiling.

The rats were trained to use the MWM 1 week before the surgery. The MWM trials comprised 2 stages; that is, the spatial acquisition trial, and the probe trial. The spatial acquisition trial required 5 consecutive days for learning. For each training trial, each rat was carefully placed in the water near the pool's edge with its head facing the wall. The rat had 60 seconds to find the platform in the southwest quadrant. Once on the platform, the rat was allowed to remain on it for 15 seconds. If the rat did not locate the platform within 60 seconds, it was led to it, and allowed to remain on it for 15 seconds. The rat was then taken from the water and placed in a holding cage for 60 seconds after each trial. Each of the 4 training trials had a different start quadrant location, and the sequence of the start quadrant positions changed each day. The rat was then towel-dried after testing and returned to its cage. The probe trial was performed the day before the surgery and 3 and 14 days after the surgery. The hidden platform was removed before the probe trial, but the surrounding visual cues were preserved. Each rat was placed in a start quadrant position that was opposite to that of the previously trained position and permitted to swim for a full minute. The rat was towel-

dried and returned to its cage after 60 seconds.

RNA-sequencing analysis

The rats were euthanized 3 and 14 days after surgery, their brain tissues were isolated, and hippocampal tissues were extracted. These sections were flash-frozen at −80 ℃ for further analysis. On postoperative day 3, the total RNA was isolated from the tissues using Trizol (Invitrogen, Carlsbad, CA, USA). For the library preparation, polyA was enriched from the total RNA as previously described (34). After the library preparation and sample pooling, Illumina sequencing was performed using Illumina HiSeq (Illumina, USA). Initially, in-house Perl scripts were used to handle the FASTQ-formatted raw data (raw reads). The clean data (clean reads) were acquired by deleting adapter reads, reads with >3 N and reads with > 20% nucleotides, and Qphred ≤5. All the downstream analyses used the ribosomal RNA-free data. Paired-end clean reads were used in the alignment process, and Hisat2 (35) and Feature count (36) were used to count the number of reads mapped to each gene. The differential expression analysis was performed with EdgeR (37). The P values were modified using Benjamini and Hochberg's method to control the false discovery rate. Genes with a |log2 (fold change)| value >1 and a q value <0.05 were considered DEGs. The top GO package and the KOBAS (38) package were used to implement the Gene Ontology (GO) and Kyoto Encyclopedia of Genes and Genomes (KEGG) enrichment analyses of the differentially expressed gene (DEG) sets.

Quantitative proteomics study and the trypsin digestive process

A proteomic analysis was performed using the tandem mass tag (TMT)-based labelling method as previously described (39). A high-intensity ultrasonic processor extracted the proteins from the hippocampus tissue samples in lysis solution (8M urea, 1% protease inhibitor) 3 days after the surgery. The residual debris was eliminated by 10 minutes of centrifugation at 12,000 g and 4 ℃. A bicinchoninic acid kit was used to measure the protein concentration.

For the trypsin digestion, the protein solution was diluted with dithiothreitol at 56 ℃ for 30 minutes before being treated with iodoacetamide at 37 ℃ for 15 minutes in the dark. The protein samples were then diluted with millimolar triethylammonium bicarbonate (TEAB) until the urea concentration was <2 M. Finally, trypsin was added at a mass ratio of 1:50 for the first digestion at 37 ℃ overnight, then 1:100 for the second digestion.

The TMT labeling process and the liquid chromatography-tandem mass spectrometry analysis

The peptides were then desalted and vacuum-dried on the Strata X C18 SPE column following the completion of the trypsin digestion process. After reconstituting in 0.5 M of TEAB, the peptides were tagged according to the instructions of the TMT kit.

The sodium/iodide symporter sources were applied to the peptides after separation. Tandem mass spectrometry (MS/MS) was done on Q Exactive Plus (Thermo Fisher Scientific, Waltham, MA, USA) equipment connected online to an ultra-performance liquid chromatography system. At 70,000 mass resolutions, complete peptides were identified using 2.0 kV electrospray (MS scan range, 350–1,600 m/z). The collected data were processed using a data-dependent scanning program. To minimize the repetitive scanning of the precursor ions, the automatic gain control was set to 50,000, with a signal threshold of 5,000 ions/second, a maximum of 200 seconds, and a dynamic exclusion time of the tandem mass scan of 15 seconds.

Bioinformatics analysis

The "limma" package was used to conduct the differential expression analysis of the proteomics. The P values were modified using Benjamini and Hochberg's method to control the false discovery rate. A fold change value >1 and a P value <0.05 were used to identify the differentially expressed proteins. Both Hemel 1.0 and GraphPad9.0 were used to analyze the heat map.

Western blot

Proteins (30 μg) from samples were boiled in Laemmli loading buffer for 5 minutes before being transferred to 0.2-m polyvinylidene-fluoride membranes (Millipore Corporation, Burlington, MA, USA) using 10% SDS-polyacrylamide gels. The blots were then treated overnight with the following antisera: β-actin (1:2,000; GB11001, Servicebio, Wuhan, China), glyceraldehyde-3-phosphate dehydrogenase (GAPDH; 1:3,000; AB-M-M001 Good Here Biotech, Hangzhou, China), coiled-coil-helix-coiled-coil-helix domain containing 3 (ChChd3; 1:1,000; 68259-1-Ig, Proteintech, Wuhan, China), PTEN induced putative kinase 1 (PINK1; 1:1,000; 23274-1-AP, Proteintech, Wuhan, China), Parkin (GB113802, Servicebio, Wuhan, China), Beclin 1 (1:1,000; GB112053, Servicebio, Wuhan, China), p62 (1:1,000; GB11239-1, Servicebio, Wuhan, China), interleukin (IL)-1β (1:1,000)

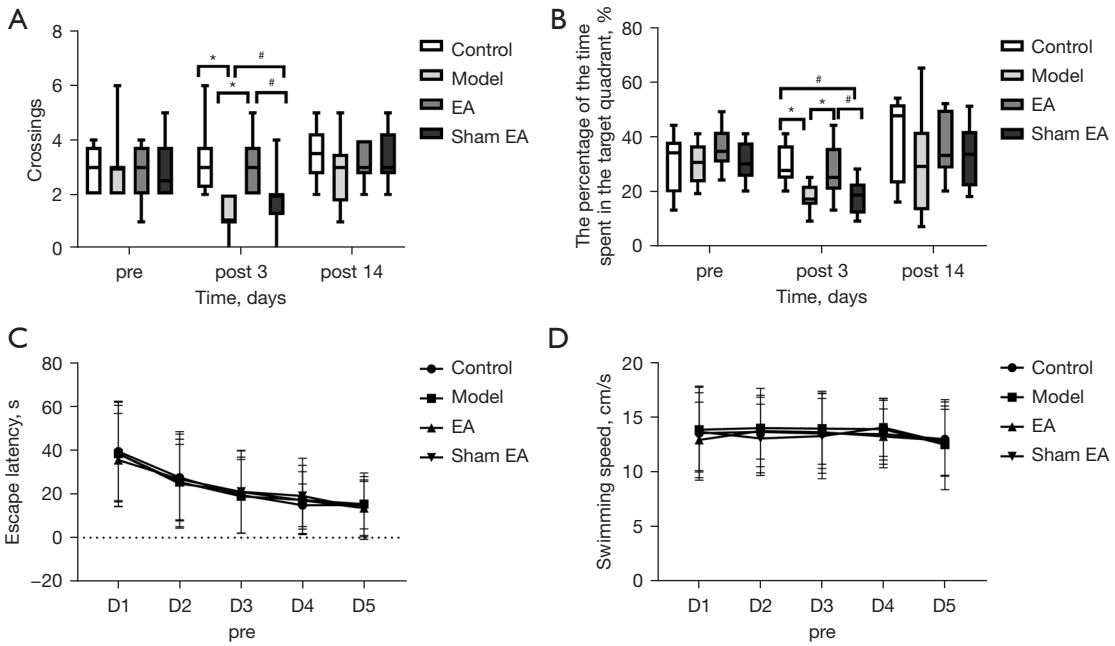

Figure 2 EA prevented surgery-induced spatial memory deficits in rats tested in the MWM. The rats in the model group made fewer platform crossings (A) and spent less time in the target quadrant (B) at 3 days, but not 14 days postoperatively than the rats in the control group. Surgery did not significantly affect the escape latency (C) or swimming speed (D) of the rats. The data were analyzed using a 2-way ANOVA (repeated measure) with Tukey's multiple comparisons test, with N=12 per group. The box plots depict the median (line) and the 25th and 75th percentiles. The whiskers extend from the 10th to the 90th percentile. #, P<0.05; *, P<0.01. Pre, the day before surgery; Post, postoperative day; EA, electroacupuncture; MWM, Morris Water Maze; ANOVA, analysis of variance.

(66737-1-Ig, Proteintech, Wuhan, China) antibodies at 4 ℃. The blots were visualized using a horseradish peroxidase-conjugated goat anti-rabbit immunoglobulin G (1:3,000) (GB23303, Servicebio, Wuhan, China) and an enhanced chemiluminescence detection system, (Millipore Corporation).

Biochemical investigation

The ROS levels were evaluated using H2DCFDA (DCFH-DA) fluorescent probes in a ROS Assay Kit (S0033S, Beyotime, Shanghai, China). The adenosine triphosphate (ATP) levels were measured according to the instructions of the kit (S0026, Beyotime, Shanghai, China). To analyze the activity of mitochondrial complex V, the mitochondria were extracted from the tissue using a Tissue Mitochondria Isolation Kit (C3606, Beyotime, Shanghai, China). The complex V activity of the mitochondria was quantified spectrophotometrically in accordance with the instructions of the detection kit (G0849W, Grace Biotechnology, Suzhou, China) and standardized to the protein content (nmol/min/mg protein).

Statistical analysis

SPSS software, version 18.0, was used to analyze all the data (SPSS, Inc., Chicago, IL, USA). The quantitative data are presented as the mean ± standard deviation. The cognitive performances of the rats in the MWM training phases were analyzed using a 2-way analysis of variance (ANOVA) (repeated measure). The experimental group and training day were taken as sources of variance of spatial memory, and the Bonferroni test was used for the post-hoc comparisons. One-way ANOVAs were performed for the probe test, biochemical index, and western immunoblots, and Newman-Keul's test was used for the *post-hoc* comparisons. A P value <0.05 was set as the accepted level of significance.

Results

The effect of EA on the spatial memory of the PND rats

In Experiment I, compared to the control group, the number of platform crossings in the model group and the sham EA group decreased significantly 3 days after surgery (P<0.01, *Figure 2A*).

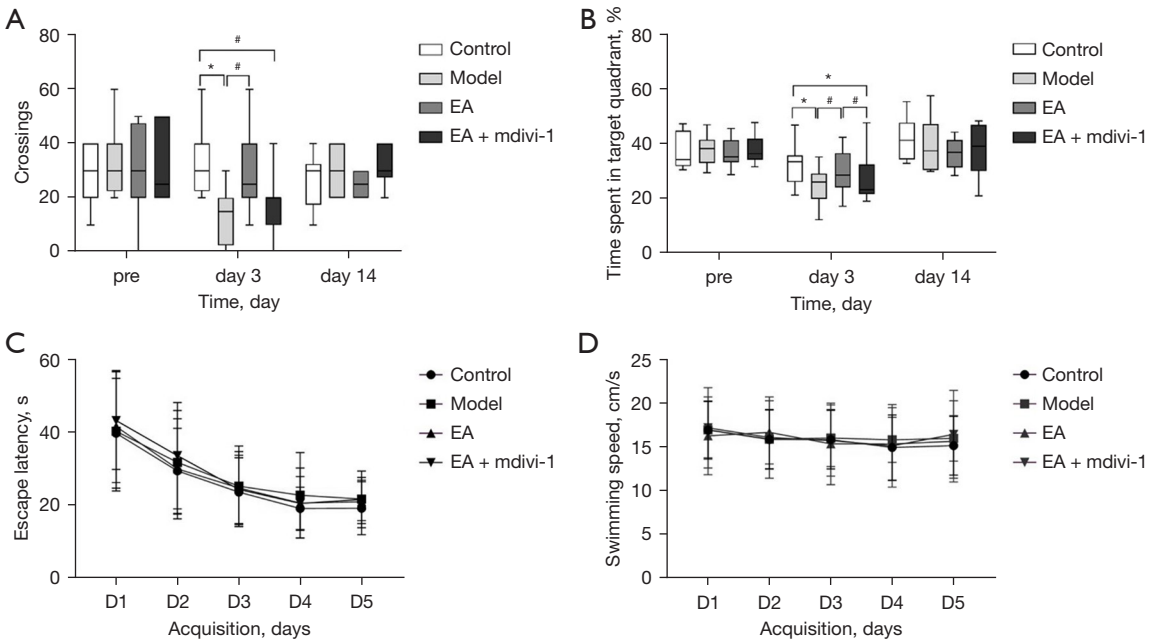

Figure 3 The protective effect of EA was reversed by the mitophagy inhibitor mdivi-1 in the MWM. The rats in the EA group made more platform crossings (A) and spent less time in the target quadrant (B) at 3 days, but not 14 days after surgery than the rats in the model group. The protective effect of EA was reversed by mdivi-1 (A,B). Surgery and mdivi-1 administration did not significantly affect the escape latency (C) or swimming speed (D) of the rats. The data were analyzed using a 2-way ANOVA (repeated measure) with Tukey's multiple comparisons test, with N=12 per group. The box plots depict the median (line) and the 25th and 75th percentiles. The whiskers extend from the 10th to the 90th percentile. #, P<0.05; *, P<0.01. Pre, the day before surgery; EA, electroacupuncture; MWM, Morris Water Maze; ANOVA, analysis of variance.

On postoperative day 3, the model group spent significantly less time in the target quadrant than the control group (P<0.01, *Figure 2B*). EA improved the decrease in the number of surgery-induced platform crossings (P<0.05, *Figure 2A*) and the time spent in the target quadrant (P<0.05, *Figure 2B*). As *Figure 2C,2D* show, the rats in all the groups did not differ significantly in terms of the platform location or swimming speed during the platform training. In Experiment II, the EA-induced protective effect on spatial memory was reversed by mdivi-1 (see *Figure 3A,3B*). There were no differences among the groups in terms of the platform location and swimming speed during the platform training (*Figure 3C,3D*). In both the experimental I and experimental II, there were no significant differences among the groups on postoperative day 14 (P>0.05). No rats died in any of the groups.

The effect of EA on the transcriptome profiles in the hippocampus of the PND rats

To investigate gene expression changes in the hippocampus underlying the spatial memory deficits and the effect of the EA treatment, we performed RNA-sequencing and screened the DEGs between the control, model, and EA groups (which comprised 3 rats per group). The edgeR package was used for the differential expression analysis. The resulting P values were adjusted using the Benjamini and Hochberg's approach to control the false discovery rate. Genes with a |log2 (fold change)| value >1 and a q value <0.05 were considered DEGs. According to the above-mentioned cut-off criteria, the expression levels of 563 DEGs in the model group were significantly altered compared to the control group (*Figure 4A*); and the expression levels of 431 DEGs in the EA group were significantly altered compared to the model group (*Figure 4B*). After parallel clustering the DEGs in the 3 groups, we found that the expression levels of 177 DEGs changed in the model group relative to the control group, but these genes tended toward normal in the EA group (*Figure 4C*). The GO analysis revealed that these 177 DEGs (*Figure 4D*) were significantly enriched in the developmental process, localization, cellular response to

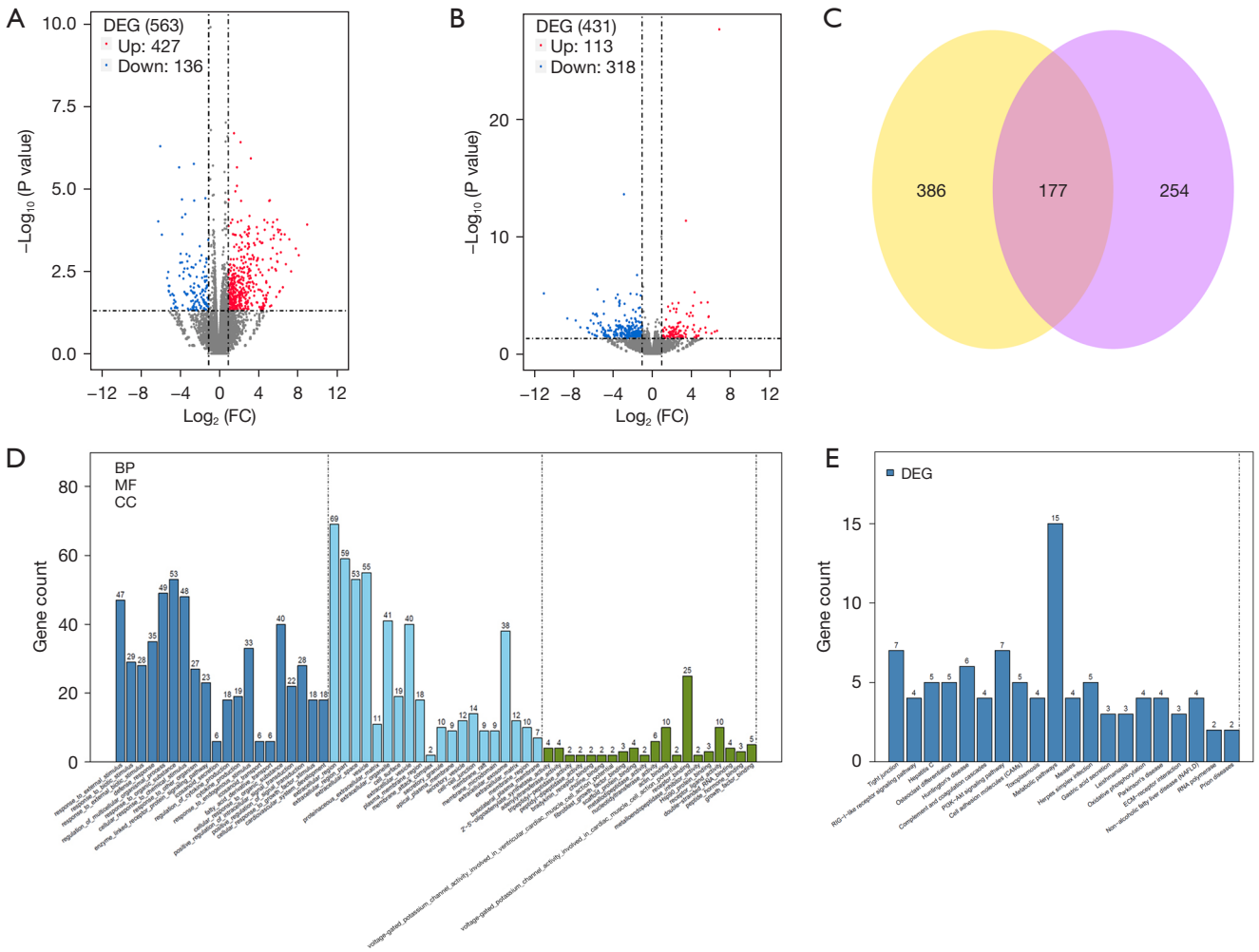

Figure 4 Gene expression data of the hippocampus of the EA-treated rats. (A,B) Volcano plot of the gene expression profiles showing significant differences between the model group *vs.* the control group, and the EA group *vs.* the model group. The genes were represented as dots, where the down-regulated genes were denoted in blue, up-regulated genes were denoted in red, and non-significant genes were denoted in gray. (C) A Venn diagram showing the significantly altered genes. There were 563 different genes between the control group and the model group. A total of 431 genes differed significantly between the EA group and the model group. Both the model group and the EA group regulated a total of 177 genes. (D,E) The GO and KEGG analyses of 177 genes were screened out by special rules (N=3 per group, criteria: fold change >1, and P<0.05). DEG, differential expressed gene; FC, fold change; GO, Gene Ontology; KEGG, Kyoto Encyclopedia of Genes and Genomes; BP, biological process; MF, molecular function; CC, cellular component; ECM, extracellular matrix; EA, electroacupuncture.

a stimulus, extracellular region, and protein binding. The KEGG analysis showed that these genes were abundant in the metabolic and phosphatidylinositol 3-kinase (PI3K)/protein kinase B (AKT) signaling pathways (*Figure 4E*).

The effect of EA on the hippocampal proteomes of the PND rats

The hippocampal samples were also tested for overall protein identification using a TMT-based proteomic analysis to understand the mechanisms of EA therapy in cognitive function (3 rats per group). A total of 4,108 proteins were identified based on the data from individual replicates (*Figure 5A,5B*). The filter criteria were as follows: a fold change value >1, and a P value <0.05. A total of 280 proteins differed between the model and control groups. In addition, 48 proteins differed significantly between the EA and model groups. When parallel

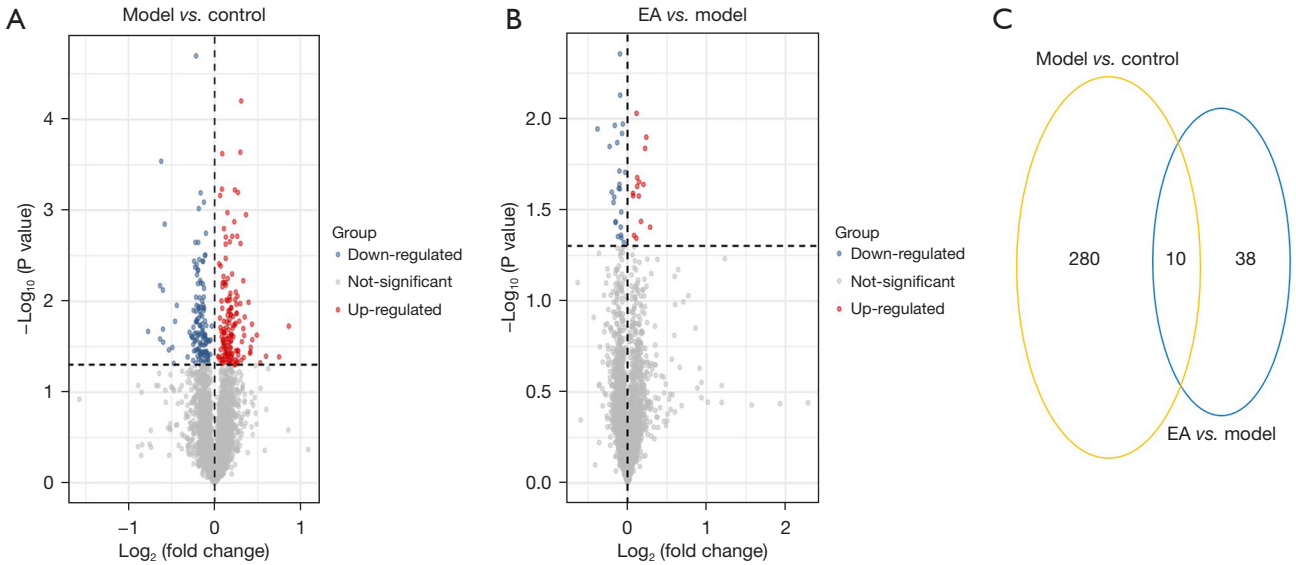

Figure 5 Protein expression data of the hippocampus of the EA-treated rats. (A) A total of 280 proteins differed between the control group and the model group. (B) A total of 48 proteins differed between the EA group and the model group. (C) A Venn diagram showing the significantly altered protein. (N=3 per group, criteria: fold change >1, and P<0.05). EA, electroacupuncture.

Table 1 Differential expression analysis of the proteins in the hippocampus associated with the EA intervention

Protein	Description	Fold change		P value		Gene name
		Model	EA	Model	EA	
MICOS complex subunit Mic19	Component of the MICOS complex	1.0929	0.93628	0.002356	0.0044035	*CHCHD3*
ESCRT-II complex subunit VPS36	Component of the ESCRT-II	0.84761	1.1036	0.0036446	0.026593	*VPS36*
Core protein II	Mitochondrion inner membrane protein	1.0508	0.98032	0.0041064	0.019692	*UQCRC2*
ATP-sensitive inward rectifier potassium channel 10	Potassium buffering action of glial cells in the brain	1.1921	0.88489	0.013655	0.028859	*KCNJ10*
Paralemmin-1	Plasma membrane dynamics and cell process formation	1.0767	0.94295	0.0203	0.03939	*PALM*
Arginine and glutamate-rich protein 1	Post-translational modification	0.91774	1.0889	0.030367	0.021076	*ARGLU1*
Probable ATP-dependent RNA helicase DDX46	Plays an essential role in splicing	1.0575	0.93803	0.04819	0.0074238	*DDX46*

EA, electroacupuncture; ATP, adenosine triphosphate; MICOS, mitochondrial contact site and cristae organizing system; ESCRT, endosomal sorting complex required for transport.

clustering the differential expressed proteins in the three groups, we found the expression levels of 10 differential expressed proteins changed in the model group relative to the control group, while these genes tended toward normal in the EA group (*Figure 5C*). Of the 10 proteins identified, 5 were upregulated in the model group, while 2 proteins were downregulated (the criteria were set as a fold change value >1, and a P value<0.05) (*Table 1*).

Identifying and verifying differentially expressed proteins

We then screened the proteins using the unique screening methods described above. ChChd3 showed the most significant difference among the 7 proteins (model *vs.*

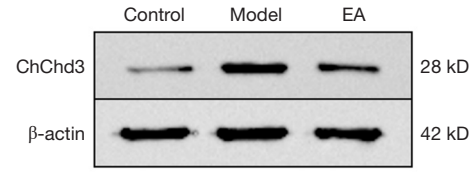

Figure 6 Western blot analysis of ChChd3 expression in each group. The ChChd3 levels were lower in the control and EA groups than the model group on postoperative day 3 (N=3 per group). EA, electroacupuncture.

control, P=0.002356; EA *vs.* model, P=0.0044035; *Table 1*). In addition, the ChChd3 level in the hippocampus was quantified by Western blotting from 3 biological replicates. The expression of ChChd3 was lower in the control and EA groups than the model group (*Figure 6*).

EA treatment reduced hippocampal oxidative stress

On postoperative day 3, the amount of ATP did not differ significantly among the 4 groups (*Figure 7A*). The ROS levels in the model group and the mdivi-1 + EA group were significantly elevated compared to the control and EA groups (*Figure 7B*). The amount of mitochondrial respiratory chain complex V activity did not differ significantly among the 4 groups (*Figure 7C*). On postoperative day 14, the amount of ATP (*Figure 7D*), the ROS levels (*Figure 7E*) and the amount of mitochondrial respiratory chain complex V activity (*Figure 7F*) did not differ significantly among the 4 groups.

EA treatment enhanced autophagy/mitophagy

As *Figure 8* shows, compared to the control group, the expression of the autophagy/mitophagy markers PINK1, Parkin, LC3, and Beclin1 was significantly decreased in the hippocampus, and IL-1β expression was significantly increased in the model group on postoperative day 3. These abnormal changes were reversed by the EA treatment. However, mdivi-1 significantly blocked the effect of EA (*Figure 8A*). At postoperative day 14, there were no significant differences between the groups (*Figure 8B*). These results indicated that improvements in spatial memory resulting from EA treatment might have been partly related to the regulation of mitophagy marker expression in the rat PND model.

Discussion

We established a PND rat model using surgical resection of the hepatic apex to explore the role of EA in the treatment of spatial memory deficits. Our results suggested that EA ameliorates the postoperative spatial memory deficits of the rats. This effect may be correlated with enhancing the autophagy and downregulating the level of ROS and the inflammatory marker IL-1β in the hippocampus after surgery.

Consistent with previous studies (20,40-42), we found that the EA group was quite similar to the control group in terms of postoperative spatial memory, which suggests that the EA treatment improved surgery-induced spatial memory loss significantly on postoperative day 3 (*Figures 2,3*). To further examine the molecular mechanisms of a suggested EA-induced protective effect on spatial memory, we analyzed the hippocampus transcriptomic and proteomic changes among the 3 groups after surgery. A total of 119 genes and 7 proteins were identified and screened. The KEGG pathway analysis revealed that these genes were related to the metabolic and PI3K-AKT signaling pathways. Based on these findings, ChChd3 related to mitochondrial morphology was screened. ChChd3 is an abundant protein and essential for maintaining the mitochondrial cristae structure (43). The loss of ChChd3 leads to crystal remodeling, perinuclear clustering, and mitochondrial fragmentation, and alterations to the cristae and an increase in mitophagy (44). The current western blot results indicated that the expression level of ChChd3 was significantly more upregulated in the model group than the control group, and the trend was reversed in the EA group.

The PI3K/AKT signaling pathway regulates proliferation, apoptosis, and autophagy during oxidative stress (45). The process of mitophagy, which is a form of selective autophagy, is necessary for the maintenance of healthy mitochondria (46). Defective or damaged mitochondria will contribute to ROS formation and release pro-apoptotic proteins into the cytoplasm if not removed, leading to cell death (47). Mitophagy might selectively remove ROS-impaired mitochondria, lowering ROS levels while maintaining normal function (48).

PINK1/Parkin signaling pathway plays an important role in autophagy activation and the formation of early autophagosome precursor structures (21). PINK1 acts a molecular sensor of mitochondrial physiology, and triggers the signal of mitophagy initiation, recruitment of Parkin to damaged mitochondria. Parkin acts an enhancer of

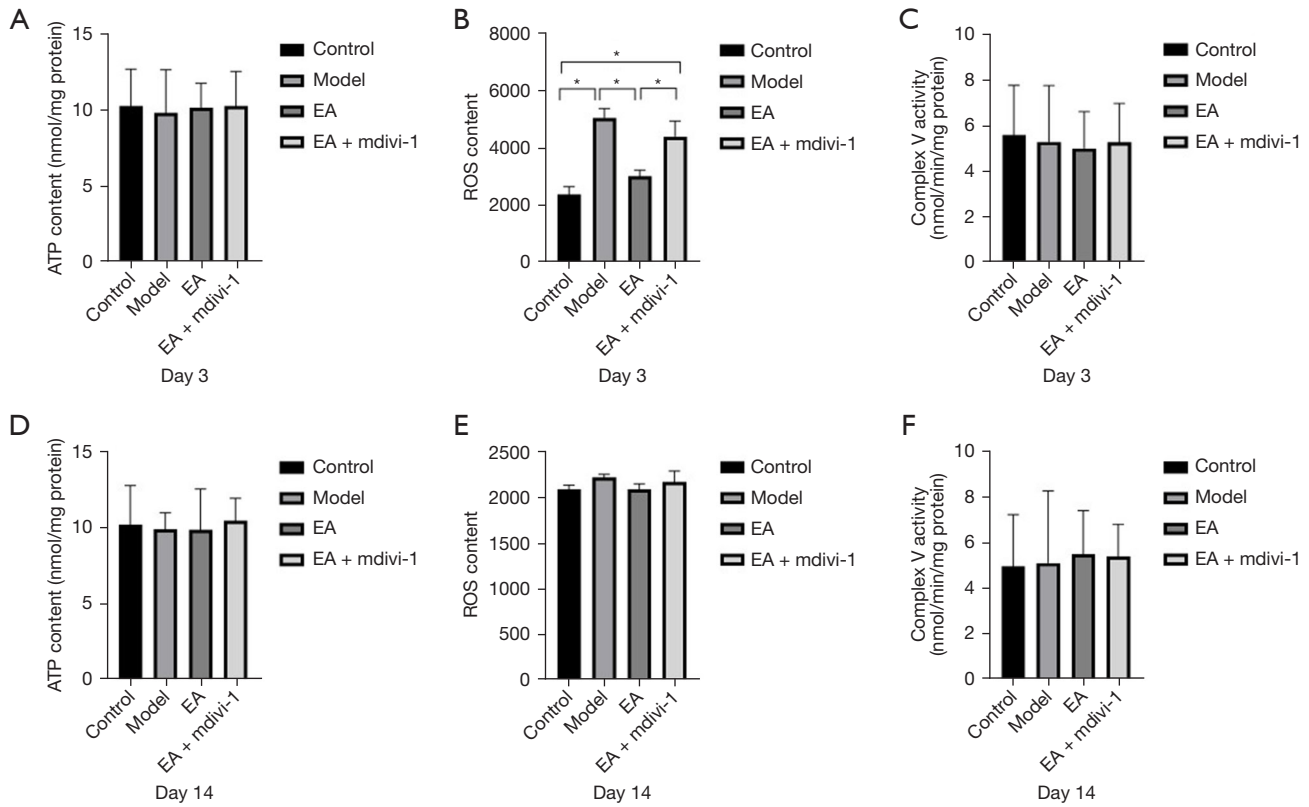

Figure 7 EA alleviated oxidative stress in the hippocampus. The biochemical investigation showed the expression of ATP content (A,D), ROS content (B,E), and the activities of mitochondrial respiratory chain complex V (C,F) in the hippocampus 3 and 14 days after surgery. The data were analyzed using a 1-way ANOVA and Tukey's test. The data are expressed as mean ± SEM (N=6, *, P<0.01). ATP, adenosine triphosphate; EA, electroacupuncture; ROS, reactive oxygen species; ANOVA, analysis of variance; SEM, standard error of the mean.

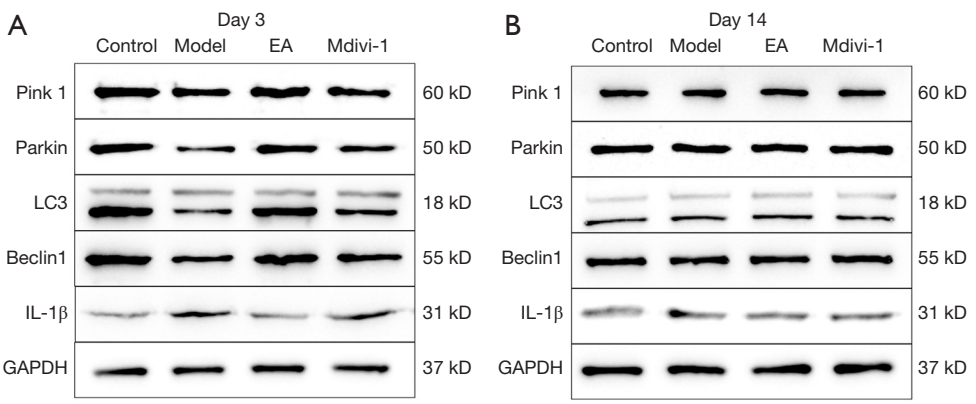

Figure 8 Immunoblot of markers for autophagy/mitophagy and inflammation. On postoperative day 3, surgery-induced impaired autophagy/mitophagy and increased inflammation (A). On postoperative day 14, there was no significant change in the protein expression levels (B) (N=3 per group). EA, electroacupuncture; IL, interleukin; GAPDH, glyceraldehyde 3-phosphate dehydrogenase.

the mitophagy signal, and amplify the ubiquitin signal of mitochondrial proteins (49). Mdivi-1 is a mitophagy inhibitor. A recent study demonstrated that the levels of mitophagy-related protein PINK1 and Parkin were reduced by Mdivi-1 treatment in neural mitochondria (50). In our study, we found that EA treatment not only improved surgery-induced spatial memory deficits but also reversed the expression of ROS and IL-1β levels in the hippocampus of the PND rats. However, these responses were inhibited by the mitophagy inhibitor Mdivi-1, which suggests that autophagy-related proteins could be key targets for reducing the incidence of PND. Decreased autophagic function leads to an accumulation of ROS, which is the activator of the Nod-like receptor protein 3 (NLRP3) inflammasome (51,52). NLRP3 catalyzes the activation of caspase-1, thereby promoting the maturation of pro-IL-1β (53). Suppressing the production of IL-1β alleviates cognitive impairment after surgery (54). Our findings are in line with those of other studies. For example, Hsu *et al.* reported that EA reduced Parkinson's disease motor symptoms and promoted autophagy and mitophagy in the substantia nigra, striatum, hippocampus, and cortical neurons of mice (55). Zhong *et al.* reported that EA treatment protected rats from cognitive impairment caused by stroke by enhancing mitophagy and inhibiting ROS-induced NLRP3 inflammasome activation (56). Collectively, our study indicated that surgery trauma inhibited mitophagy activation in rat hippocampus, and the neuroprotection provided by mitophagy may result from the removal of damaged mitochondria.

Mitochondria are the prime source for the production of reactive species (9), and the mitochondrial ATP synthase is a multiprotein complex that generates ATP from adenosine diphosphate and phosphate ion (57). Thus, the respiratory chain complex is most susceptible to free radical damage, and the activity of ATP synthase is reduced as a consequence of oxidative damage (58). Defective mitochondria can be hazardous, as they produce excess ROS, which weakens the assembly of ATP with ATP synthase, and interfere with metabolic processes (16). Mitochondrial energy deficit and reduced enzyme activity contribute to aging and neurological diseases (59). However, we did not replicate these findings in this study. The ATP levels and the activities of the mitochondrial respiratory chain complex V did not differ significantly between the 4 groups at each time point. This may be because the degree of oxidative stress was not severe enough to alter ATP production (60). We thus speculate that a significant increase in oxidative stress is only relevant when the damage is severe enough to have an effect on mitochondrial ATP synthase.

This study had several limitations. First, we only relied on concomitant changes of EA rather than precise mechanisms. Second, quantitative polymerase chain reaction should have been conducted on day 3 to verify the RNA-sequencing data. Third, no gene knockout was used, so we do not know whether the expression of ChChd3 in our model is directly associated with memory impairment or whether EA treatment can improve the surgical phenotype by regulating the ChChd3 protein. Finally, we did not evaluate the extent of mitophagy (e.g., autophagosome) with imaging techniques, such as cellular immunofluorescence labelling. Thus, further research needs to be conducted to answer such questions.

Conclusions

Our findings indicated that the surgery-induced spatial memory deficits in rats could be effectively alleviated by the treatment with EA. The underlying mechanism may involve the inhibition of ROS and IL-1β expression by modulating the PINK1/Parkin-mediated mitophagy pathway in the hippocampus.

Acknowledgments

Funding: This work was supported by the National Natural Science Foundation of China (grant Nos. 81671076 and 82072086).

Footnote

Reporting Checklist: The authors have completed the ARRIVE reporting checklist. Available at https://atm.amegroups.com/article/view/10.21037/atm-22-6262/rc

Data Sharing Statement: Available at https://atm.amegroups.com/article/view/10.21037/atm-22-6262/dss

Conflicts of Interest: All authors have completed the ICMJE uniform disclosure form (available at https://atm.amegroups.com/article/view/10.21037/atm-22-6262/coif). All authors report that this work was supported by the National Natural Science Foundation of China (grant Nos. 81671076 and 82072086). The authors have no other

conflicts of interest to declare.

Ethical Statement: The authors are accountable for all aspects of the work in ensuring that questions related to the accuracy or integrity of any part of the work are appropriately investigated and resolved. This study was approved by the Ethical Committee of the Aviation General Hospital (No. HK-2019-12-17). All the animal experiments were performed in accordance with the National Institutes of Health Guidelines for the Care and Use of Laboratory Animals.

References

1. Evered LA, Goldstein PA. Reducing Perioperative Neurocognitive Disorders (PND) Through Depth of Anesthesia Monitoring: A Critical Review. Int J Gen Med 2021;14:153-62.
2. Evered L, Silbert B, Knopman DS, et al. Recommendations for the nomenclature of cognitive change associated with anaesthesia and surgery-2018. Br J Anaesth 2018;121:1005-12.
3. Lai Z, Min J, Li J, et al. Surgery Trauma Severity but not Anesthesia Length Contributes to Postoperative Cognitive Dysfunction in Mice. J Alzheimers Dis 2021;80:245-57.
4. Fan CH, Peng B, Zhang FC. The postoperative effect of sevoflurane inhalational anesthesia on cognitive function and inflammatory response of pediatric patients. Eur Rev Med Pharmacol Sci 2018;22:3971-5.
5. Safavynia SA, Goldstein PA. The Role of Neuroinflammation in Postoperative Cognitive Dysfunction: Moving From Hypothesis to Treatment. Front Psychiatry 2018;9:752.
6. Shertzer HG, Krishan M, Genter MB. Dietary whey protein stimulates mitochondrial activity and decreases oxidative stress in mouse female brain. Neurosci Lett 2013;548:159-64.
7. Boz Z, Hu M, Yu Y, et al. N-acetylcysteine prevents olanzapine-induced oxidative stress in mHypoA-59 hypothalamic neurons. Sci Rep 2020;10:19185.
8. Ma D, Zheng B, Liu HL, et al. Klf5 down-regulation induces vascular senescence through eIF5a depletion and mitochondrial fission. PLoS Biol 2020;18:e3000808.
9. Netto MB, de Oliveira Junior AN, Goldim M, et al. Oxidative stress and mitochondrial dysfunction contributes to postoperative cognitive dysfunction in elderly rats. Brain Behav Immun 2018;73:661-9.
10. Ye Z, Fang B, Pan J, et al. miR-138 suppresses the proliferation, metastasis and autophagy of non-small cell lung cancer by targeting Sirt1. Oncol Rep 2017;37:3244-52.
11. Fassio A, Falace A, Esposito A, et al. Emerging Role of the Autophagy/Lysosomal Degradative Pathway in Neurodevelopmental Disorders With Epilepsy. Front Cell Neurosci 2020;14:39.
12. Yuan H, Wang X, Hill K, et al. Autophagy attenuates noise-induced hearing loss by reducing oxidative stress. Antioxid Redox Signal 2015;22:1308-24.
13. Chen Y, Zhang P, Lin X, et al. Mitophagy impairment is involved in sevoflurane-induced cognitive dysfunction in aged rats. Aging (Albany NY) 2020;12:17235-56.
14. Wang Y, Xiong H, Liu D, et al. Autophagy inhibition specifically promotes epithelial-mesenchymal transition and invasion in RAS-mutated cancer cells. Autophagy 2019;15:886-99.
15. Guan ZF, Zhou XL, Zhang XM, et al. Beclin-1- mediated autophagy may be involved in the elderly cognitive and affective disorders in streptozotocin-induced diabetic mice. Transl Neurodegener 2016;5:22.
16. Youle RJ, van der Bliek AM. Mitochondrial fission, fusion, and stress. Science 2012;337:1062-5.
17. Lin JG, Chen CJ, Yang HB, et al. Electroacupuncture Promotes Recovery of Motor Function and Reduces Dopaminergic Neuron Degeneration in Rodent Models of Parkinson's Disease. Int J Mol Sci 2017;18:1846.
18. Li X, Dai Q, Shi Z, et al. Clinical Efficacy and Safety of Electroacupuncture in Migraine Treatment: A Systematic Review and Network Meta-Analysis. Am J Chin Med 2019;47:1755-80.
19. Ho YS, Zhao FY, Yeung WF, et al. Application of Acupuncture to Attenuate Immune Responses and Oxidative Stress in Postoperative Cognitive Dysfunction: What Do We Know So Far? Oxid Med Cell Longev 2020;2020:9641904.
20. Liu PR, Cao F, Zhang Y, et al. Electroacupuncture reduces astrocyte number and oxidative stress in aged rats with surgery-induced cognitive dysfunction. J Int Med Res

2019;47:3860-73.
21. Wang H, Chen S, Zhang Y, et al. Electroacupuncture ameliorates neuronal injury by Pink1/Parkin-mediated mitophagy clearance in cerebral ischemia-reperfusion. Nitric Oxide 2019;91:23-34.
22. An J, Fang Q, Huang C, et al. Deeper total intravenous anesthesia reduced the incidence of early postoperative cognitive dysfunction after microvascular decompression for facial spasm. J Neurosurg Anesthesiol 2011;23:12-7.
23. Fang Q, Qian X, An J, et al. Higher dose dexamethasone increases early postoperative cognitive dysfunction. J Neurosurg Anesthesiol 2014;26:220-5.
24. Niu K, Qin JL, Lu GF, et al. Dexmedetomidine Reverses Postoperative Spatial Memory Deficit by Targeting Surf1 and Cytochrome c. Neuroscience 2021;466:148-61.
25. Andersen SL. Trajectories of brain development: point of vulnerability or window of opportunity? Neurosci Biobehav Rev 2003;27:3-18.
26. Ghaffary S, Ghaeli P, Talasaz AH, et al. Effect of memantine on post-operative cognitive dysfunction after cardiac surgeries: a randomized clinical trial. Daru 2017;25:24.
27. Deyu H, Luqing C, Xianglian L, et al. Protective mechanisms involving enhanced mitochondrial functions and mitophagy against T-2 toxin-induced toxicities in GH3 cells. Toxicol Lett 2018;295:41-53.
28. Ma J, Williams J, Eastwood D, et al. High-dose Propofol Anesthesia Reduces the Occurrence of Postoperative Cognitive Dysfunction via Maintaining Cytoskeleton. Neuroscience 2019;421:136-43.
29. Yin CS, Jeong HS, Park HJ, et al. A proposed transpositional acupoint system in a mouse and rat model. Res Vet Sci 2008;84:159-65.
30. Chen Y, Zhao Y, Luo DN, et al. Electroacupuncture Regulates Disorders of Gut-Brain Interaction by Decreasing Corticotropin-Releasing Factor in a Rat Model of IBS. Gastroenterol Res Pract 2019;2019:1759842.
31. Wan Y, Wilson SG, Han J, et al. The effect of genotype on sensitivity to electroacupuncture analgesia. Pain 2001;91:5-13.
32. Zhang X, Yan H, Yuan Y, et al. Cerebral ischemia-reperfusion-induced autophagy protects against neuronal injury by mitochondrial clearance. Autophagy 2013;9:1321-33.
33. Jarrard LE. On the role of the hippocampus in learning and memory in the rat. Behav Neural Biol 1993;60:9-26.
34. Alam SG, Zhang Q, Prasad N, et al. The mammalian LINC complex regulates genome transcriptional responses to substrate rigidity. Sci Rep 2016;6:38063.
35. Kim D, Langmead B, Salzberg SL. HISAT: a fast spliced aligner with low memory requirements. Nat Methods 2015;12:357-60.
36. Liao Y, Smyth GK, Shi W. featureCounts: an efficient general purpose program for assigning sequence reads to genomic features. Bioinformatics 2014;30:923-30.
37. Robinson MD, McCarthy DJ, Smyth GK. edgeR: a Bioconductor package for differential expression analysis of digital gene expression data. Bioinformatics 2010;26:139-40.
38. Bu D, Luo H, Huo P, et al. KOBAS-i: intelligent prioritization and exploratory visualization of biological functions for gene enrichment analysis. Nucleic Acids Res 2021;49:W317-25.
39. Guerra-Moreno A, Isasa M, Bhanu MK, et al. Proteomic Analysis Identifies Ribosome Reduction as an Effective Proteotoxic Stress Response. J Biol Chem 2015;290:29695-706.
40. Sun L, Yong Y, Wei P, et al. Electroacupuncture ameliorates postoperative cognitive dysfunction and associated neuroinflammation via NLRP3 signal inhibition in aged mice. CNS Neurosci Ther 2022;28:390-400.
41. Liu PR, Zhou Y, Zhang Y, et al. Electroacupuncture alleviates surgery-induced cognitive dysfunction by increasing α7-nAChR expression and inhibiting inflammatory pathway in aged rats. Neurosci Lett 2017;659:1-6.
42. Feng PP, Deng P, Liu LH, et al. Electroacupuncture Alleviates Postoperative Cognitive Dysfunction in Aged Rats by Inhibiting Hippocampal Neuroinflammation Activated via Microglia/TLRs Pathway. Evid Based Complement Alternat Med 2017;2017:6421260.
43. Guan R, Chen Y, Zeng L, et al. Oncosis-inducing cyclometalated iridium(iii) complexes. Chem Sci 2018;9:5183-90.
44. Darshi M, Mendiola VL, Mackey MR, et al. ChChd3, an inner mitochondrial membrane protein, is essential for maintaining crista integrity and mitochondrial function. J Biol Chem 2011;286:2918-32.
45. Wang H, Liu Y, Wang D, et al. The Upstream Pathway of mTOR-Mediated Autophagy in Liver Diseases. Cells 2019;8:1597.
46. Kim I, Rodriguez-Enriquez S, Lemasters JJ. Selective degradation of mitochondria by mitophagy. Arch Biochem Biophys 2007;462:245-53.
47. Wang Y, Liu N, Lu B. Mechanisms and roles of mitophagy in neurodegenerative diseases. CNS Neurosci Ther

2019;25:859-75.
48. Fan P, Xie XH, Chen CH, et al. Molecular Regulation Mechanisms and Interactions Between Reactive Oxygen Species and Mitophagy. DNA Cell Biol 2019;38:10-22.
49. Eldeeb MA, Ragheb MA. N-degron-mediated degradation and regulation of mitochondrial PINK1 kinase. Curr Genet 2020;66:693-701.
50. Nhu NT, Li Q, Liu Y, et al. Effects of Mdivi-1 on Neural Mitochondrial Dysfunction and Mitochondria-Mediated Apoptosis in Ischemia-Reperfusion Injury After Stroke: A Systematic Review of Preclinical Studies. Front Mol Neurosci 2021;14:778569.
51. Razani B, Feng C, Coleman T, et al. Autophagy links inflammasomes to atherosclerotic progression. Cell Metab 2012;15:534-44.
52. Zhou R, Yazdi AS, Menu P, et al. A role for mitochondria in NLRP3 inflammasome activation. Nature 2011;469:221-5.
53. Chan EWL, Krishnansamy S, Wong C, et al. The NLRP3 inflammasome is involved in the neuroprotective mechanism of neural stem cells against microglia-mediated toxicity in SH-SY5Y cells via the attenuation of tau hyperphosphorylation and amyloidogenesis. Neurotoxicology 2019;70:91-8.
54. Cibelli M, Fidalgo AR, Terrando N, et al. Role of interleukin-1beta in postoperative cognitive dysfunction. Ann Neurol 2010;68:360-8.
55. Hsu WT, Chen YH, Yang HB, et al. Electroacupuncture Improves Motor Symptoms of Parkinson's Disease and Promotes Neuronal Autophagy Activity in Mouse Brain. Am J Chin Med 2020;48:1651-69.
56. Zhong X, Chen B, Li Z, et al. Electroacupuncture Ameliorates Cognitive Impairment Through the Inhibition of NLRP3 Inflammasome Activation by Regulating Melatonin-Mediated Mitophagy in Stroke Rats. Neurochem Res 2022;47:1917-30.
57. Cha MY, Cho HJ, Kim C, et al. Mitochondrial ATP synthase activity is impaired by suppressed O-GlcNAcylation in Alzheimer's disease. Hum Mol Genet 2015;24:6492-504.
58. Reed T, Perluigi M, Sultana R, et al. Redox proteomic identification of 4-hydroxy-2-nonenal-modified brain proteins in amnestic mild cognitive impairment: insight into the role of lipid peroxidation in the progression and pathogenesis of Alzheimer's disease. Neurobiol Dis 2008;30:107-20.
59. Chaturvedi RK, Flint Beal M. Mitochondrial diseases of the brain. Free Radic Biol Med 2013;63:1-29.
60. Baratli Y, Charles AL, Wolff V, et al. Age modulates Fe3O4 nanoparticles liver toxicity: dose-dependent decrease in mitochondrial respiratory chain complexes activities and coupling in middle-aged as compared to young rats. Biomed Res Int 2014;2014:474081.

(English Language Editor: L. Huleatt)

Cite this article as: Guo J, Niu K, Ma BF, Sun LN, Fang QW, An JX. Electroacupuncture ameliorates surgery-induced spatial memory deficits by promoting mitophagy in rats. Ann Transl Med 2023;11(2):74. doi: 10.21037/atm-22-6262

